Optical manipulation and characterisation of aerosol particles using a single-beam gradient force optical trap

Laura Mitchem and Jonathan P. Reid

Received 18th December 2007
First published as an Advance Article on the web 4th February 2008
DOI: 10.1039/b609713h

The application of optical tweezers (a single-beam gradient force optical trap) to the manipulation and characterisation of aerosol particles is discussed in this *tutorial review*. Optical tweezers allow not only the indefinite control over a single droplet, but control over arrays of particles. Typical particle sizes span the 1–10 μm diameter range. When coupled with spectroscopic techniques for probing evolving particle size (with nanometre accuracy), composition, phase and mixing state, detailed investigations of the thermodynamic properties of aerosol, the kinetics of particle transformation, and the nature of interparticle forces and coagulation can be undertaken.

I. Introduction

Aerosols play a role in a wide range of scientific disciplines ranging from atmospheric chemistry and physics, combustion science and dusty plasmas, to drug delivery and epidemiology. For example, they influence the climate through absorption and scattering of incoming and outgoing radiation, directly influencing the radiative balance of the atmosphere. Aerosol is a multiphase system composed of solid or liquid particles suspended within a gas phase. The two phases are coupled, with changes in the composition or temperature of the gas phase affecting the behaviour of the condensed phase particles. Aerosol particles are typically in the size range of a few nanometers to tens of microns, and can be multiphase or multicomponent, with the composition at the droplet surface varying significantly from the bulk.

To understand the chemical and physical properties of aerosol, the condensed phase and gas phase must be well characterised along with the interphase coupling. Particle size, composition, phase and morphology influence the partitioning of components between the gas and condensed phase. These properties, along with the composition and temperature of the gas phase must be characterised, preferably *in situ*, to understand the fundamental properties governing aerosol processes. Conventionally, the chemical and physical properties of aerosol are investigated by performing ensemble measurements on a macroscopic aerosol sample under controlled environmental conditions. However, the results of such studies are characterised by averaging over distributions of particle size and composition. Consequently any measurement provides an average estimate of the property of the aerosol under investigation.[1] From these studies it is impossible to infer the size, composition, mixing state and morphology of a single particle.

Coupling techniques for manipulating aerosol particles with optical techniques for particle characterisation allows the chemical and physical properties of aerosols to be interrogated directly and *in situ*. Laser techniques for probing non-intrusively the size, composition, temperature and refractive index of the aerosol particle allow the fundamental properties influencing the particle behaviour to be characterised. Additionally, aerosol particles can be trapped indefinitely allowing the gas phase to be varied and the evolving particle to be monitored as it responds to the environmental change. This

School of Chemistry, University of Bristol, Bristol, UK BS8 1TS

Jonathan Reid received his undergraduate and post-graduate degrees from the University of Oxford (MA, DPhil) before moving to a post-doctoral fellowship at JILA, University of Colorado, USA. In 2000 he took up a lectureship at the University of Birmingham, moving to the University of Bristol in 2004. He is currently a Reader in Physical Chemistry and an EPSRC Advanced Research Fellow. He was awarded the 2001 Harrison Memorial Prize and the 2004 Marlow Medal by the Royal Society of Chemistry.

Laura Mitchem received her MChem degree from the University of Leeds in 1999, moving to the Department of Instrumentation and Analytical Science, UMIST, to undertake her graduate research. In 2003 she was awarded her PhD, which focused on optical beam and infrared spectroscopic techniques for measuring drug diffusion in skin mimetics. After a brief period of postdoctoral research at UMIST, she moved to the University of Bristol in 2004 to apply optical tweezers to studies of aerosol dynamics.

permits direct investigation of the coupling between the gas phase and condensed phase.

Conventionally, the isolation of individual aerosol particles has been accomplished through electrostatic trapping, optical levitation or the use of an acoustic trap. When coupled with elastic and inelastic light scattering techniques, electrostatic trapping has been used to investigate the evaporation of liquid droplets,[2] the thermodynamic properties of aerosol including particle phase,[3,4] and the uptake of gas phase constituents on a single particle.[5] A variety of electrode designs have been explored, including two parallel ring electrodes, four parallel disc electrodes, hemispherical end-cap electrodes coupled with a toroidal electrode, and a double-ring double-disk configuration.[2] Each design has both advantages and disadvantages, offering differing degrees of positional stability for particles within the 1–100 μm diameter range, and varying extents of optical access. Typically, a trapped particle must be charged to thousands of elementary charge units, depending on the particle mass, size and the potential applied to the electrodes. Single particles can be manipulated indefinitely, although fine control over multiple particles is not possible. A cloud of charged particles may adopt an equilibrium configuration governed by interparticle coulomb repulsions.

Acoustic traps have also been used to examine the evaporation kinetics of liquid droplets and the phase behaviour of aerosol droplets, notably allowing access to particles with sizes at the millimetre length scale.[6] Measurements of the optical properties of single particles, including ice covered carbon particles, have been performed by coupling a FTIR spectrometer to an acoustic trap.[7] The variable pressure and temperature of the surrounding gas phase arising from the strong acoustic fields required to levitate a particle must be rigorously accounted for in any interpretation of mass and heat transfer.[6] Multiple aerosol particles can be studied simultaneously by capturing droplets in different nodes of the acoustic standing wave.

Optical levitation uses the optical scattering force exerted by radiation pressure to counterbalance the gravitational force acting on a particle.[8,9] By fine adjustment of the laser power, the evolving mass and size of a liquid droplet tens of microns in diameter can be followed allowing thermodynamic measurements of equilibrium particle size and phase.[10] Measurements have also been made of the resonance absorption accompanied by an associated change in droplet temperature.[11]

In this publication we review the application of a single-beam gradient-force optical trap (optical tweezers) to the manipulation of single and multiple aerosol particles. Although this approach has some similarity to optical levitation, the trapping mechanism relies instead on the dominance of the optical gradient force, produced by a tightly focused laser beam, over the scattering force, which dominates in a more loosely focused Gaussian beam.[12,13] In comparison to the broad range of electrostatic, optical and acoustic levitation techniques described above, aerosol optical tweezers allow the routine manipulation of multiple particles simultaneously, forming arrays of aerosol particles using holographic optical tweezers. Further, particles smaller than 10 μm can be isolated for indefinite timescales and particles smaller than 1 μm have been sampled. Particles can be positioned with high accuracy relative to each other permitting investigations of interparticle interactions. The force constant of the gradient-force trap provides stability against external perturbations, such as gas flow or bombardment by other aerosol particles. The high collection efficiency of inelastically scattered light can allow the acquisition of spectra with excellent signal-to-noise on timescales shorter than 1 second from sample volumes that are typically only picolitres.

In this review, we will first describe the principles of aerosol manipulation using optical tweezers. This will be followed by a discussion of the spectroscopic techniques that have been used to probe trapped aerosol particles. In the final section, we will describe a range of applications that have been explored using aerosol optical tweezers.

II. Principles of aerosol manipulation

II.a Optical tweezing of single aerosol droplets

When a particle interacts with a highly focused laser beam it experiences two forces, the scattering force and the gradient force. The mechanism by which a spherical particle is trapped is dependent upon the interplay of these two forces. The electric field polarises the spherical particle and generates an induced dipole that has a magnitude that depends on the polarisability, α, of the particle; this induced dipole is proportional to the difference between the refractive indices of the particle, n_p, and surrounding medium, n_m, and the volume of the particle. The scattering force, defined by eqn (1), is proportional to the square of the induced dipole, is directly proportional to the intensity of the incident laser beam and acts in the direction of beam propagation, as shown schematically in Fig. 1.[12]

$$F_{scat} \approx \alpha^2 E^2 \approx (n_p - n_m)^2 r^6 I \quad (1)$$

E is the electric field amplitude, r is the radius of the particle and I is the intensity of the laser beam.

The gradient force arises from a spatially varying field, such as that occurring at a laser focus. This leads to a net force exerted on the induced dipole which is directly proportional to the gradient in light intensity created by the tightly focused laser beam. The gradient force acts to draw the particle towards the region of highest light intensity. In the systems used for optical tweezing studies, this region is the focal point of a microscope objective, and the force is defined by

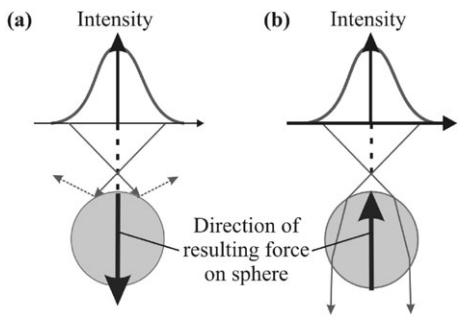

Fig. 1 Illustration of the action of the (a) scattering and (b) gradient forces acting on a spherical transparent particle.

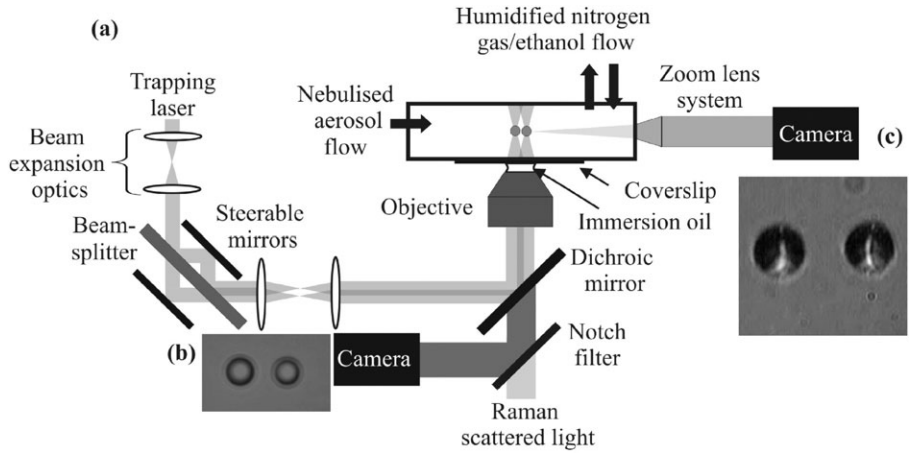

Fig. 2 (a) Experimental schematic of the dual trapping optical tweezers system. [Reprinted with permission from ref. 34. Copyright 2006 Elsevier.] (b) In-plane image of two optically trapped NaCl/aqueous aerosol droplets collected using conventional brightfield microscopy. (c) Side-image of two optically trapped NaCl/aqueous aerosol droplets collected using the zoom lens system mounted perpendicular to the trapping beam.

$$F_{\text{grad}} \approx (\alpha/2)\nabla E^2, \qquad (2)$$

where ∇ is the differential operator.[12]

The scattering and gradient forces act in opposition, with the former pushing the particle along the direction of beam propagation and away from regions of high light intensity, while the latter draws the particle along the light intensity gradient into the most intense region of the beam. For the gradient force to act in this way, the refractive index of the particle must exceed that of its surroundings. A stable three-dimensional trap is created when the gradient force acting on the particle dominates the scattering force. The coupling of the scattering and gradient forces results in a stable axial trapping position just beyond the focal point of the objective.[13] The particles trapped using optical tweezers are micron-sized in diameter, exceeding the wavelength of the trapping beam. As such, they are in the Mie scattering regime. Ray optics can be used to describe their behaviour.[13]

When held in a gradient force optical trap a particle experiences a restoring force, piconewtons in magnitude, which acts to restrain the particle to an equilibrium position at the region of greatest light intensity.[13] The particle can be considered to behave as a simple harmonic oscillator and, for small displacements from the equilibrium trapping position, the restoring force is a linear function of particle displacement.[14] The existence of a restoring force allows direct manipulation of the trapped particle, with the gradient force pulling the particle back to its equilibrium position and retaining it in the trap even when external perturbations are applied. This property offers advantages over simple optical levitation techniques by allowing the direct investigation of interparticle interactions and accurate control over particle position.

Fig. 2(a) shows a schematic of an optical tweezers system used to trap aerosol particles in air. At a trapping wavelength of 532 nm the complex refractive index of water is at a minimum,[1] ensuring no droplet heating occurs.[15] The 532 nm trapping beam passes through two sets of beam expansion optics and is focused through a coverslip by a 100× oil immersion objective (with a numerical aperture, NA, of 1.25) creating the optical trap within a specially designed stainless steel cell. The high NA objective maximises the gradient forces acting on the trapped particle ensuring stable trapping. Aerosol, generated using a medical ultrasonic nebuliser, is introduced into the cell *via* a side port and an aerosol droplet is trapped directly from the aerosol flow. Aerosol droplets of 4–14 μm diameter can be trapped using laser powers of 5–15 mW.[15]

The relative humidity (RH) experienced by the trapped aerosol is controlled by varying the flow rate of humidified nitrogen gas into the cell. However, aerosol droplets are typically doped with sodium chloride, reducing their vapour pressure, and allowing equilibration with the subsaturated RH of their environment.[15] Once trapped, an aerosol droplet can be held indefinitely, the conditions of the environment surrounding the droplet can be varied and the response of the size, phase and composition monitored.

The trapped aerosol droplet is imaged in two ways. An in-plane image of the droplet, as shown in Fig. 2(b), is collected using conventional brightfield microscopy. The droplet is imaged using the focused light of a blue LED, which is collected by the objective and imaged using a CCD camera.[16] A side-image of the trapped droplet, as shown in Fig. 2(c), is collected using a zoom lens system with an overall magnification of 45.72×, mounted perpendicular to the trapping beam.[17] Illumination is provided by a white light source, and again the image is collected using a CCD camera. The in-plane and side-imaging allow simultaneous monitoring of the lateral and axial positions of the optically trapped aerosol droplet.

The efficiency of trapping is defined by the dimensionless efficiency, Q.[13,15]

$$F = \frac{n_{\text{m}} PQ}{c} \qquad (3)$$

F defines the optical forces acting on the particle, P is the power of the incident laser beam and c is the speed of light. Q, which characterises the effectiveness of the laser beam in exerting an optical force on the trapped particle, is dependent on the refractive indices of the particle and surroundings, the profile of the incident beam, the NA of the objective and the

position of the trapped particle with respect to the beam focus.[18]

The optical forces experienced by a trapped particle can be resolved into axial and lateral forces. The axial trapping efficiency, defined by eqn (4), can be determined by measuring the minimum incident laser power required to counterbalance the gravitational force acting on the particle while retaining the particle within the trap.[18,19]

$$Q_{\text{axial}} = \frac{4}{3}\pi r^3 \rho g \cdot \frac{1}{n_{\text{m}} P/c} \qquad (4)$$

ρ is the density of the particle and g the gravitational acceleration. Trapping efficiencies are in the range 0 to 1 and values of 0.10 ± 0.04 and 0.45 ± 0.12 have been measured for water and decane droplets trapped in air, with powers as low as 1 mW commonly required to retain a droplet in the optical trap.[15] These values are comparable to those measured in liquids.[13]

The forces acting along the axis of propagation of the laser beam have been investigated by exploring the laser power dependence of the height of a trapped NaCl/aqueous aerosol droplet with respect to the coverslip surface above which it is trapped.[17] With increasing trapping power, the droplet was observed to shift to a higher trapping position above the coverslip. This shift results from a change in the coupling between the scattering and gradient forces acting on the particle. Additionally, as the droplet increased in size the particle was observed to sit at a lower trapping position, closer to the coverslip. This decrease in height is a result of the greater gravitational force acting on the particle. The interplay of the gravitational, scattering and gradient forces is therefore shown to change with particle weight and geometric cross-section, and the power of the trapping beam.[17]

The Brownian dynamics of an optically trapped aqueous aerosol droplet have been used to investigate the influence of viscous damping on the motion of a trapped particle.[20] In liquids, the viscosity of the solvent dampens the Brownian motion of a particle and the motion can be considered to be over-damped. For aerosol droplets, the magnitude of the viscous damping provided by the surrounding gas phase is considerably lower. Di Leonardo *et al.* monitored the displacement of an aerosol droplet from its equilibrium position and observed a transition between an over-damped regime at low trapping power and an under-damped regime at high trapping power. Further, the axial displacement of the droplet was observed to exceed the displacement in the lateral direction indicating weaker trapping along the direction of laser propagation. This difference is a result of aberrations created by the microscope objective.

II.b Trapping of multiple aerosol droplets

The simultaneous creation of multiple optical traps allows direct interrogation of the fundamental factors influencing the coagulation and mixing state of aerosol particles, and also offers the potential for characterising multiple aerosol particles simultaneously. Multiple trapping studies in the liquid phase are principally focused on force measurements and studies of interparticle interactions.[13] The creation of multiple traps for studying aerosol particles in the gas phase is achieved using identical techniques to those used in the liquid phase.

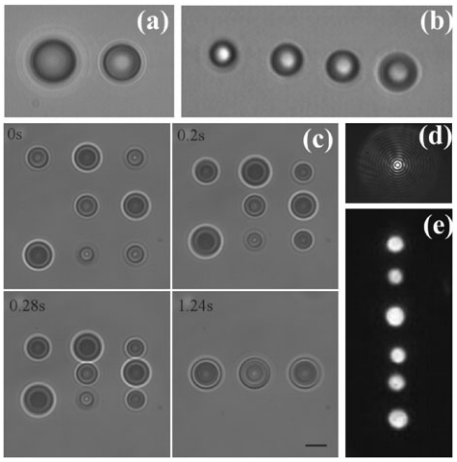

Fig. 3 (a) Dual trapping of a decane droplet (right) and a NaCl/aqueous aerosol droplet. (b) Simultaneous trapping of 4 NaCl/aqueous aerosol particles using an AOM. [Reproduced with permission from ref. 23. Copyright 2006 American Institute of Physics.] (c) Trapping of 8 aerosol droplets using a HOT array and subsequent manipulation to coagulation in $\sim$1 second resulting in a single row of 3 composite droplets. [Reproduced with permission from Ref. 27. Copyright 2008 Royal Society of Chemistry.] (d) Bessel beam intensity profile. (e) Trapping of 6 dodecane droplets within the central Bessel core.

In the simplest form, multiple traps are created following the procedure detailed by Fallman *et al.*, which involves the insertion of a 50 : 50 beam splitter at the conjugate plane to the beam expansion optics in the single optical tweezers set-up. This creates two single beam gradient-force optical traps, as shown in Fig. 2(a),[21] which are independently controllable allowing the trapping and manipulation of two aerosol droplets simultaneously. Trapping two aerosol droplets of differing composition and steering the traps together can allow studies of droplet coagulation. For example, a water droplet can be trapped in one trap and a decane droplet in the other, as shown in Fig. 3(a). By steering the two droplets together the mixing state of the resultant droplet can be investigated directly.[22]

Acousto-optic modulation of the trapping beam has also been used to create multiple aerosol traps, with up to four aerosol droplets being trapped simultaneously, as shown in Fig. 3(b).[23] An acousto-optic modulator (AOM) creates multiple traps by scanning the laser beam rapidly between a specified number of sites. Each trapping site is defined a dwell time, typically between 1 and 10 ms, and the AOM steers the trapping beam between these sites on a sub-100 μs timescale.[23,24] When trapping multiple aerosol particles, the scanning beam must return to each trapping position within 10 ms to guarantee that the trapped particle is not lost by sedimentation onto the coverslip before the optical restoring force is re-applied.[23]

The range over which the optical forces are experienced by a trapped droplet has been investigated by translating the trapping site over increasing distances and measuring the maximum distance at which a trapped droplet was able to

follow the trapping position and be recaptured before sedimenting out.[23] At displacements of a few microns the droplet was shown to encounter a strong restoring force and was recaptured at the new trap position. However, as the distance of translation was increased to ~6–9 μm, the droplet was no longer recaptured. The maximum recapture distance was found to be droplet size and laser power dependent.

While multiple aerosol droplets can be captured and manipulated using dual trapping and AOM techniques, the trapping of arrays of aerosol particles can be achieved using holographic optical tweezers (HOTs).[25] HOTs modify the relative phase of the light across the trapping beam wavefront producing desired patterns defined by the user. These patterns can be simple single spots used to trap single aerosol droplets, complex arrays used to trap multiple aerosol droplets, as shown in Fig. 3(c), or complex beam types such as Laguerre–Gaussian.[26,27] The trapping of arrays of aerosol droplets using the HOT system can allow the sampling and characterisation of multiple aerosol droplets simultaneously, permitting comparative studies on different aerosol particles.

Burnham *et al.* have used HOT arrays, up to 40 μm by 40 μm in dimension, to trap multiple aerosol droplets simultaneously.[26,27] An example of a 30 μm by 30 μm array is shown in Fig. 3(c). The array, composed of 9 optical traps equally spaced on a square grid, was loaded by dosing the traps with a flow of nebulised NaCl/aqueous aerosol droplets.[27] 3.5–6 μm size particles were captured and the size was found to increase with the power of each optical trap. The trapping efficiency was found to be comparable to that measured for the single trap optical tweezers system.[15] An example of the spatial control of the aerosol array that is achievable is illustrated by studies of the coagulation of multiple aerosol droplets shown in Fig. 3(c).[27] Eight aerosol droplets were captured using a 3×3 HOT array. The square array was collapsed into a single row of 3 droplets within ~1 second, illustrating the real time control of aerosol coagulation possible with HOTs.

II.c Other optical techniques for manipulating aerosol

A range of other optical techniques can also be exploited for aerosol manipulation. The controlled transfer or guiding of aerosol particles over a distance of millimetres is possible using a Bessel beam. A Bessel beam has a non-diffracting central core, as illustrated by the intensity profile shown in Fig. 3(d), along which trapped particles can propagate a distance of millimetres.[28] Once a particle is trapped within the central core, the beam reconstructs around the trapped particle and this can lead to the simultaneous trapping of multiple particles along the direction of beam propagation. An example of six dodecane droplets trapped within the Bessel core is shown in Fig. 3(e). The separation distance at which particles are located is dependent on the size of the particle around which the beam must reconstruct.[29]

If the beam is propagating vertically, the equilibrium position at which a particle resides is determined by the interplay of the gravitational force acting on the particle and the radiation pressure of the central Bessel core. By varying the radiation pressure (*i.e.* the laser power) it is possible to guide the particle along the central core. McGloin *et al.* have trapped and guided water droplets over millimetres using a beam with a central core diameter of 4 μm,[27] a distance more than ten times that possible using a Gaussian beam. The optical guiding of aerosol particles using a Bessel beam can potentially be used to characterise multiple particles simultaneously. By trapping a particle and varying the power of the central core it would be possible to drive the particle sequentially though a number of spectroscopic probe beams in a controlled manner.[24]

The trapping and optical guiding of multiple aerosol particles is also possible using a dual beam fibre trap, as demonstrated by McGloin *et al.*[27] Aqueous aerosol droplets, 3–7 μm in diameter, were trapped by counter-propagating beams emerging from two aligned multimode fibres. In this technique, the trapping is governed by the radiation pressure of these aligned beams, with approximately 100 mW of power required from each fibre. By varying the power in one fibre with respect to the other, it is possible to translate the trapped particle over distances up to 50 μm between the fibres. Additionally, the multimode nature of the fibres results in the generation of multiple equilibrium trapping positions known as 'hot spots' within different horizontal planes between the fibres. This property allows the trapping and manipulation of multiple particles, leading to the potential use of this technique for the simultaneous sampling and characterisation of multiple aerosol particles.

III. Characterisation of optically manipulated aerosol particles using Raman spectroscopy

By coupling optical manipulation techniques, such as optical tweezers or optical levitation, with spectroscopic characterisation, the dynamic properties of aerosol particles can be determined *in situ* with high time resolution. For example, the composition, size, temperature and phase of single aerosol droplets can be investigated directly by Raman spectroscopy. The influence of inclusions and refractive index inhomogeneities on the processes occurring in aerosol can also be investigated. Raman scattering techniques have been used to characterise optically levitated liquid droplets[9,30,31] and their extension to optically tweezed aerosol droplets will now be described.

Raman scattering can be observed from a trapped aerosol droplet with the tweezing beam acting as the excitation source. The Raman scattered light is collected with high efficiency in the backward scattering geometry by the objective used to create the optical trap and imaged onto the entrance slit of a spectrograph coupled to a CCD camera. Fig. 4 shows typical Raman spectra of three optically tweezed aqueous/NaCl droplets collected using an integration time of 1 second. The spectra are composed of a broad underlying spontaneous Raman band superimposed with sharp resonance peaks arising from stimulated Raman scatter (abbreviated to SRS in what follows). Each spectrum, referred to below as a cavity enhanced Raman spectrum (CERS), provides a unique fingerprint from which the composition, phase, size and refractive index of the trapped droplet can be determined.

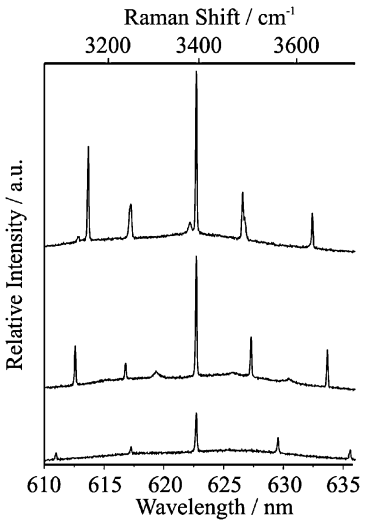

Fig. 4 CERS fingerprints of three optically trapped NaCl/aqueous aerosol droplets of differing size (5.103, 4.547 and 3.918 μm from top to bottom, respectively). The underlying spontaneous band is evident with SRS superimposed at WGM wavelengths. The experiment is performed using a 514.5 nm excitation wavelength. [Reproduced by permission of Ref. 15. Copyright 2004 PCCP Owner Societies.]

III.a Spontaneous Raman scattering

Spontaneous Raman scatter arises from the inelastic scattering of photons by the molecular components present within the aerosol, providing a fingerprint of the chemical composition of the particle. Promotion of the molecules to higher internal energy states by incident photons is accompanied by the scattering of photons with lower residual energy, referred to as Stokes scattering. Fig. 4 shows the broad spontaneous Raman band observed for an optically tweezed NaCl/aqueous aerosol droplet in air. The inelastic scattering of the trapping beam by the intramolecular OH stretching vibrations of water result in a Stokes shift of 2900–3700 cm^{-1} from the incident laser beam. The contour of the band, which has a maximum at 3480 cm^{-1} and a shoulder at 3290 cm^{-1}, reflects the distribution of intermolecular hydrogen bonding environments of water molecules present within the droplet.[16] Thus, the band shape shows a systematic dependence on ionic strength due to changes in the hydrogen-bonding network with ion concentration.[16,32] For example, an increase in the NaCl concentration of the droplet results in a greater disruption of the hydrogen bonding environment within the water phase, and as a consequence the OH stretching band peak maximum is observed to shift to higher frequencies whilst the low frequency shoulder at 3290 cm^{-1} diminishes in intensity.[16,32]

We have shown that the spontaneous Raman scatter observed from NaCl/aqueous droplets conforms to that observed from bulk samples of equivalent concentration.[16,33] This conformity demonstrates that the ionic strength of the inorganic ions present within the droplet can be determined by direct comparison of the spontaneous bands recorded from droplet and bulk phase samples. The polarisations of the incident and Raman scatter must be considered as the band contour shows a dependence upon both and the selected polarisations of the incident laser and Raman scatter must be equivalent in bulk and droplet measurements.

The shape of the OH spontaneous band also shows a dependence on the temperature of water.[16,33] An increase in temperature disrupts the hydrogen bonding network of the bulk, affecting the vibrational frequencies of the OH stretching vibrations. This disruption results in a decrease in the shoulder observed at 3290 cm^{-1}.[33] Further, the excellent correlation between the OH band contour observed for bulk water and for an optically tweezed water droplet supports the earlier conclusion of the absence of droplet heating during optical tweezers measurements.[15,16]

The use of the spontaneous intensities to monitor the changing composition of an optically trapped aerosol droplet has been investigated by exposing a trapped NaCl/aqueous aerosol droplet to a flow of ethanol vapour.[34] The initial spectrum, recorded prior to exposure, was composed of the broad spontaneous band characteristic of a water droplet. Following the introduction of ethanol vapour into the aerosol cell, a CH band was observed to appear in the region 2852–3016 cm^{-1},[34] which increased in intensity with time as the concentration of ethanol within the aqueous droplet increased. Additionally, by comparing the C–H to O–H intensity ratio with those determined from calibration measurements made on bulk samples, the composition of the droplet was determined directly.

III.b Stimulated Raman scattering

The CERS fingerprint of an optically trapped aerosol droplet provides a unique signature of droplet size in addition to composition.[30] The CERS fingerprints in Fig. 4 are obtained for three optically tweezed NaCl/aqueous aerosol droplets of differing size.[15] Each consists of a broad OH spontaneous Raman band with resonance structure superimposed, arising from stimulated Raman scattering (SRS). At discrete wavelengths, the inelastically scattered Raman light can become trapped by total internal reflection, forming a standing wave, which circulates the droplet circumference.[35,36] At these wave lengths, which are commensurate with whispering gallery modes (WGMs), the droplet behaves as a low loss optical cavity providing a mechanism for optical feedback leading to the amplification of the Raman signal. The threshold intensity for the occurrence of SRS is observed at much lower incident laser intensities for droplets than bulk samples, as a result of the ability of the droplet to act as a low loss cavity.[35,36]

The WGM wavelengths can be expressed in terms of the size parameter, x, which is determined from the radius of the particle and the wavelength of the WGM, λ.[30,32]

$$x = \frac{2\pi r}{\lambda} \tag{5}$$

By comparison of the WGM wavelengths with Mie scattering calculations the size of the optically trapped aerosol droplet can be calculated with nanometre accuracy, dependent upon the accuracy with which the WGM wavelengths and the refractive index of the droplet are known.[31,37] The accuracy of the wavelength measured is determined by the spectral dispersion of the spectrograph used to record the droplet spectra. A dispersion of 0.02 nm per pixel equates to an

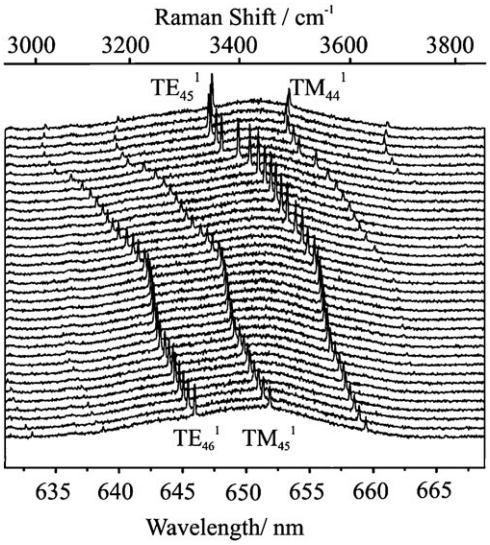

Fig. 5 Change in WGM wavelengths of a NaCl/aqueous aerosol droplet as the RH of its surroundings varies. The initial droplet size equals 3.986 μm. The droplet evaporates to a final size of 3.913 μm over a time period of 30 min. The experiment is performed using a 532 nm excitation wavelength. [Reprinted with permission from ref. 16. Copyright 2006 American Chemical Society.]

accuracy of ±2 nm in size.[16,38] Droplet sizes ranging from a few microns to several tens of microns have been probed using this technique.[32] As can be seen in the spectra in Fig. 4, the spacing between the WGMs is dependent upon droplet size, tending towards a greater separation with decrease in droplet radius.[32]

Each WGM is defined by a mode number, n, and a mode order, l.[35,37] The mode number defines the integer number of wavelengths that form the standing wave circulating the droplet circumference, whilst the mode order defines the number of maxima in the radial distribution of mode intensity. As the mode order increases the light penetrates to a greater depth within the droplet, with the maximum distance from the droplet interface estimated as $\sim r - r/n_p$.[30] The polarisation state of each WGM is also defined, with transverse electric (TE) modes possessing no radial variation in the electric field, and transverse magnetic (TM) modes possessing no radial variation in the magnetic field.[36] The mode number, mode order and polarisation have been assigned for each WGM shown in Fig. 5, with the mode number and mode order denoted by the subscript and superscript, respectively.

The uncertainty in refractive index used to calculate the droplet size is dependent upon the uncertainty in droplet composition. In the measurements described here, the refractive index of the droplet when initially trapped was assumed to equal that of the nebulised solution. This was confirmed by nebulising aerosol droplets directly onto a refractometer and measuring the refractive index of the droplets generated by the nebulisation process. Comparison of the droplet refractive index with that measured for the bulk solution, showed the values to be identical within an uncertainty of ±0.0001.[39] The variation of refractive index with solute concentration, wavelength (*i.e.* dispersion), and temperature must also be accounted for in the refractive index formulation. For NaCl/aqueous, the refractive index can be calculated with an accuracy better than 0.05% allowing the determination of the droplet radius with nanometre accuracy.[30,39]

Once an aerosol droplet is trapped it can be held indefinitely using optical tweezers, allowing investigation of the temporal variation in droplet size as it equilibrates with its surroundings. Fig. 5 shows the variation in WGM wavelengths observed during equilibration of a NaCl/aqueous aerosol droplet with the RH of the aerosol cell, illustrating the achievable time resolution and size precision.[16] Initially the droplet radius equals 3.986 μm and over a period of 30 minutes the droplet evaporates by 73 nm to a size of 3.913 μm. The shift in the resonance wavelengths to the blue is indicative of a decrease in droplet size. The change in droplet refractive index arising from the evolving composition during the evaporation is accounted for when calculating the variation in droplet size.

The intensity of the SRS observed at WGM wavelengths is related to the spontaneous band shape by an exponential scaling factor:[32]

$$I_{SRS}(\lambda) = I_0(\lambda) \exp [G(g\lambda)-1)] \quad (6)$$

$I_{SRS}(\lambda)$ is the SRS intensity, I_0 is the intensity of the spontaneous scatter at wavelength λ, G is the gain factor determining the amplification of the Raman light, and $g(\lambda)$ is the line shape function describing the spontaneous band shape. The gain factor is dependent on the intensity of the incident laser beam and the concentration of species within the sample investigated.[30] Whilst gain factors of 10–15 are typical for droplets illuminated with high intensity pulsed lasers, the gain factor observed in tweezing studies is very low, typically $\ll 1$.[16,32] Such a low gain is consistent with the spectra shown in Fig. 4 in which the WGM intensities follow closely the shape of the underlying spontaneous band contour.

The lifetime of a WGM is defined by the quality factor, Q_F.[32]

$$Q_F = \frac{2 \times \pi \times \text{Energy Stored}}{\text{Energy Lost per Cycle}} \quad (7)$$

Values of 10^5–10^8 are typical, with values in excess of 10^5 corresponding to a pathlength of meters in a droplet microns in diameter, corresponding to a WGM lifetime of nanoseconds.[30] Q_F is dependent upon droplet size, mode order and the complex refractive index of the droplet.[35] Q_F increases with increasing mode number. Therefore, as a droplet increases in size, the mode numbers of the WGMs increase and the resonance modes sharpen and increase in intensity.[40] Conversely, Q_F decreases with increase in mode order, resulting in broader resonant modes.[40] Finally, the Q_F of a TE mode exceeds that of the corresponding TM modes[34] resulting in more intense and distinguishable resonances in the CERS fingerprint.

IV. Applications of aerosol optical tweezing

To understand the properties of an aerosol particle we have shown that the evolving size, composition, phase and refractive index must be monitored. For example, an atmospheric aerosol particle will equilibrate with the RH of the surroundings and reach an equilibrium size determined by the particle

composition and the mixing state of different chemical components.[1] The coupling of optical tweezers with CERS enables time resolved studies of aerosol droplets to be performed. The independent manipulation of aerosol particles of different components allows direct investigation of the factors influencing mixing state. Some recent applications of aerosol optical tweezers will now be discussed in greater detail.

IV.a Direct investigations of the coagulation of aerosol particles

The coagulation of aerosol particles within the atmosphere influences particle size distributions and alters the mixing state of aerosol components.[1] We have performed benchmark studies of aerosol coagulation to investigate the behaviour of a composite droplet following a well-defined coagulation event. Initial studies involved the coagulation of two water droplets using dual optical tweezers.[15] The sizes of the trapped droplets were determined by alternatively steering each droplet into the Raman detection area, within the trapping region imaged by the spectrograph. This allowed collection of the CERS fingerprint of each droplet independently, assignment of their WGMs, and determination of their radii. The droplets were monitored continuously until the WGM wavelengths, and consequently the droplet sizes, had stabilised. The three dimensional nature of the optical trap formed by the tweezers allows direct manipulation of the aerosol particles, permitting control over coagulation as shown in Fig. 6(a). The combined volume of the droplets prior to coagulation was compared with that of the coagulated droplet and the two were shown to be in good agreement within an error of $\pm 3 \times 10^{-19}$ m^3, corresponding to an error of less than 0.1% in droplet volume.[23] This illustrates the accuracy with which the droplet size can be determined using CERS, with an excellent correlation found over 15 coagulation events.

The coagulation of solid aerosol particles can also be studied using optical tweezers.[41] For example, the coagulation of two NaCl/sodium dodecyl sulfate (SDS) metastable microgel particles has been studied. Fig. 6(b) shows the two microgel particles held simultaneously in two parallel optical traps. On controlled coagulation, the particles were found to adhere forming a composite conjoined particle. The traps were then separated leaving the conjoined particle in one of the traps. This procedure also demonstrates that the manipulation of non-spherical solid aerosol particles is possible using optical tweezers.

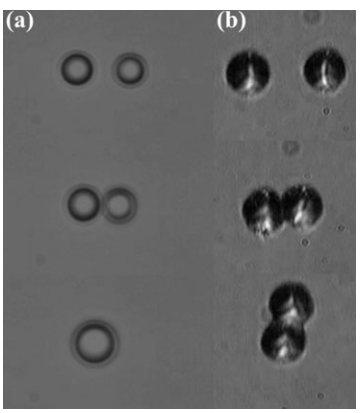

Fig. 6 (a) In-plane image illustrating the manipulation of two NaCl/aqueous aerosol droplets to the point of coagulation using dual optical tweezers. (b) Side-image showing the controlled coagulation of two sodium dodecyl sulfate/NaCl microgel particles which results in the particles adhering and forming a composite conjoined particle. [Reprinted with permission from ref. 41. Copyright 2007 American Chemical Society.]

IV.b Comparative growth and evaporation measurements

Comparison of the response of two droplets of differing composition to their surrounding gas phase allows direct investigation of the effect of droplet composition on the accommodation of a trace species. Such comparative measurements of aerosol growth can be performed on two aerosol droplets simultaneously using dual optical tweezers, allowing the effect of composition on the thermodynamic properties of an aerosol droplet to be investigated directly.

To illustrate the potential use of this technique the growth rates of two NaCl/aqueous aerosol droplets, held in parallel optical traps and exposed to ethanol vapour, have been measured by monitoring their evolving size and composition.[34] The change in composition was recorded through the appearance and increase in intensity of the CH vibrational Raman band in the region 2852–3016 cm^{-1}. Additionally, the WGM progressions were observed to extend over the OH and CH bands, confirming the formation of a homogeneous mixed component droplet of increasing size. These results demonstrated for the first time that the evolving size and composition of two droplets could be monitored simultaneously, within an identical gas phase environment. More generally, this suggested that direct comparative measurements of the effect of composition on the kinetics and thermodynamics of aerosol transformation could be made.

IV.c Comparative thermodynamic measurements

The hygroscopic properties of an aerosol define the way in which the equilibrium particle size and phase vary with the RH of the surroundings. While the hygroscopic properties of inorganic/aqueous aerosol droplets are well characterised, those of mixed organic/inorganic/aqueous aerosols are less well understood.[39] Generally, it is important to consider the behaviour of water-soluble organic components, insoluble compounds and immiscible organic phases. We review here our ability to study the equilibrium size behaviour of a benchmark system, aqueous sodium chloride aerosol, before considering the influence of organic components on the thermodynamic properties of aerosol. This will allow us to highlight the problems associated with making measurements on single particles and the value in making comparative measurements on two droplets concurrently.

The equilibrium size of an aqueous aerosol droplet is governed by its response to the RH of the surrounding gas phase, which is determined by the interaction of two competing effects, the Kelvin effect and the solute effect.[1] The Kelvin effect defines the influence of surface curvature on the vapour pressure of a droplet with that of a curved surface exceeding that of a flat surface and increasing with diminishing size. The

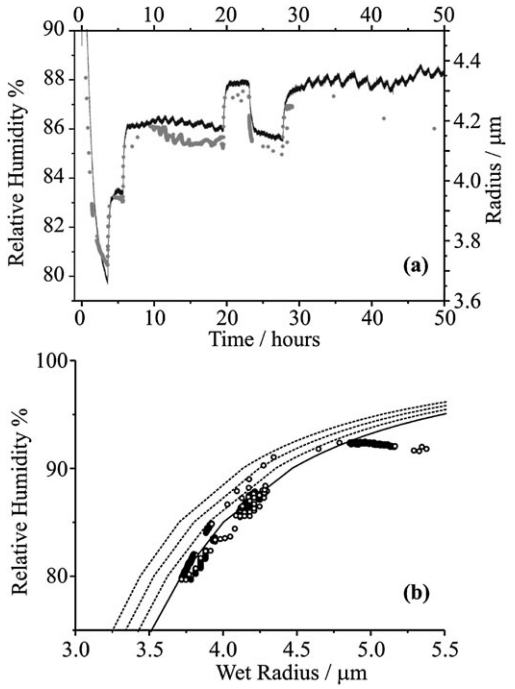

Fig. 7 (a) Variation in the equilibrium size of an aqueous NaCl droplet (grey circles) with changing RH of the surrounding environment (black line) measured using a RH capacitance probe. (b) Measured variation in wet particle size with RH (the Köhler curve) for a NaCl/aqueous aerosol droplet compared with theoretical Köhler curves calculated for solute loadings corresponding to dry particles with radii (curves from left to right) 1741, 1761, 1807 and 1803 nm (estimated to be the composition of the measurement). At early times, the measured results show a poor correlation due to the presence of RH gradients within the cell. At long times excellent agreement is observed. [Reprinted with permission from ref. 16. Copyright 2006 American Chemical Society.]

solute effect describes the lowering of the vapour pressure by solutes present within the droplet. As the RH of the gas phase decreases, the droplet evaporates and the concentration of an inorganic solute within the droplet bulk increases. This leads to a more pronounced lowering of the droplet vapour pressure. The solute and Kelvin effects counteract each other and, thus, for a droplet with a given fixed mass of involatile solute, a single equilibrium size occurs at a particular RH. Köhler theory accounts for the interplay of these two effects and is used to predict the size at which the droplet's vapour pressure equals the RH of its surroundings, and the droplet and vapour are in equilibrium.[1]

We have used optical tweezers to investigate the equilibrium size behaviour of aqueous/NaCl aerosol droplets.[16] A NaCl/aqueous aerosol droplet was trapped and the RH of its surroundings varied using a flow of humidified nitrogen gas. The evolving wet particle size was monitored using the CERS fingerprint. Fig. 7(a) shows the evolving droplet size with RH recorded over a time period of 50 hours. The RH was measured using a capacitance probe, positioned within 2 cm of the trapped droplet, with a time response of 50 seconds and an accuracy of ±2% at RHs below 90%. The oscillations in size of approximately 30 nm are a result of the laboratory air-conditioning, corresponding to a variation in the gas phase RH of approximately 0.2%.

Measurement of the variation in droplet size (wet particle size) and composition with RH allows direct evaluation of the Köhler curve of the optically trapped aerosol droplet. Fig. 7(b) displays the variation in wet particle size with measured RH, the Köhler curve for the optically trapped droplet, and compares it with theoretical Köhler curves calculated for solute loadings comparable to that estimated for the experimental droplet. Although the agreement is reasonable, the slow time response and poor accuracy of the RH measurement, particularly at RHs greater than 90%, compromise the quality of the experimental data. Additionally, RH gradients within the aerosol cell can lead to significant differences between the RH measured by the probe and the RH experienced by the droplet. It is clear that the accuracy of the size measurement is not supported by a corresponding degree of accuracy in the characterisation of the gas phase composition.

The accuracy of the RH measured can be improved by using a NaCl/aqueous droplet as a highly accurate and responsive probe of the RH of the environment, positioned in close proximity to a second droplet of interest. This is a simple extension of the comparative aerosol measurements already described. If the dry particle size of the control droplet is known and the solute is a well-characterised salt such as sodium chloride, the dependence of the wet particle size with RH can be very accurately predicted. Then, by measuring the size of the control droplet, the RH can be inferred with an accuracy estimated to be better than ±0.09%.[39] This procedure allows the gas phase RH in proximity to the second droplet to be determined with a high time response as well as high accuracy.

We have applied this strategy to examine the equilibrium size variation of aqueous sodium chloride droplets containing the water soluble organic compound glutaric acid, a typical dicarboxylic acid found in the atmosphere. The measurement involved the sequential loading of two optical traps, the first with a droplet containing sodium chloride and the organic component, and the second with a droplet containing only the inorganic salt. The droplets were held at a separation of approximately 30 μm and their size monitored as the RH within the trapping region fell from close to 100% following the loading of the traps, as shown in Fig. 8(a). The change in refractive index arising from the change in composition of the droplets during evaporation was accounted for in the size calculations.

The evolving size of the aqueous sodium chloride control droplet was used to determine the variation in RH, as described above. Once the RH variation was known, the experimental Köhler curve could be directly determined for the glutaric acid/NaCl/aqueous aerosol droplet, as shown in Fig. 8(b). In this figure, we also include the estimated Köhler curves for droplets of similar composition determined from a conventional growth factor parameterisation, which shows excellent agreement within the error bars of RH discussed above. An error in the RH of 0.1% translates into an error in the wet particle size of 2.2%.[39] This provides the first example of the comparative measurement of Köhler curves by dual trapping aerosol droplets of differing composition, allowing

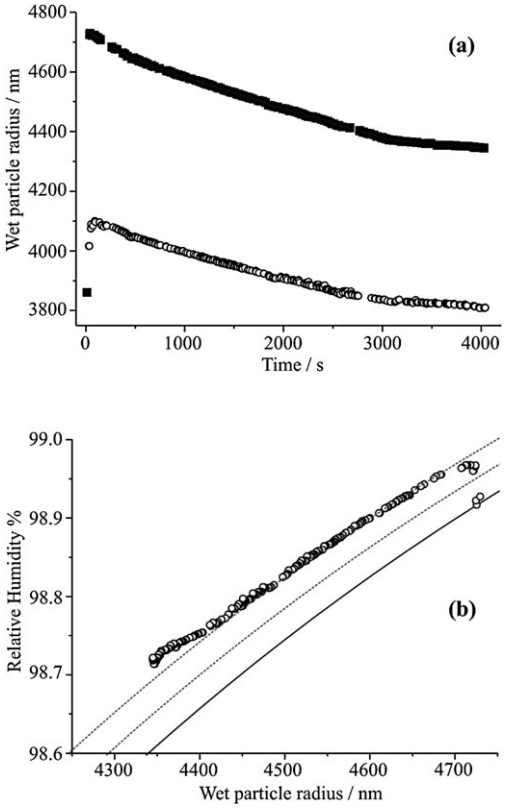

Fig. 8 (a) Variation in wet particle size of a NaCl/aqueous aerosol droplet (open circles) and a mixed glutaric acid/NaCl/aqueous aerosol droplet (filled squares) during equilibration of the RH of the surrounding environment. [Reproduced by permission from Ref. 41. Copyright 2007 American Chemical Society.] (b) Measured variation in wet particle size (circles) with RH for the mixed glutaric acid/NaCl/aqueous aerosol droplet compared with theoretical Köhler curves. The theoretical curves are calculated for a solution droplet composed of glutaric acid and NaCl with dry particle sizes of 826 and 924 nm, 836 and 934 nm, and 846 and 944 nm (estimated to be the composition of the measurement), respectively (for curves from left to right). [Reproduced by permission fromRef. 39. Copyright 2008 Royal Society of Chemistry.]

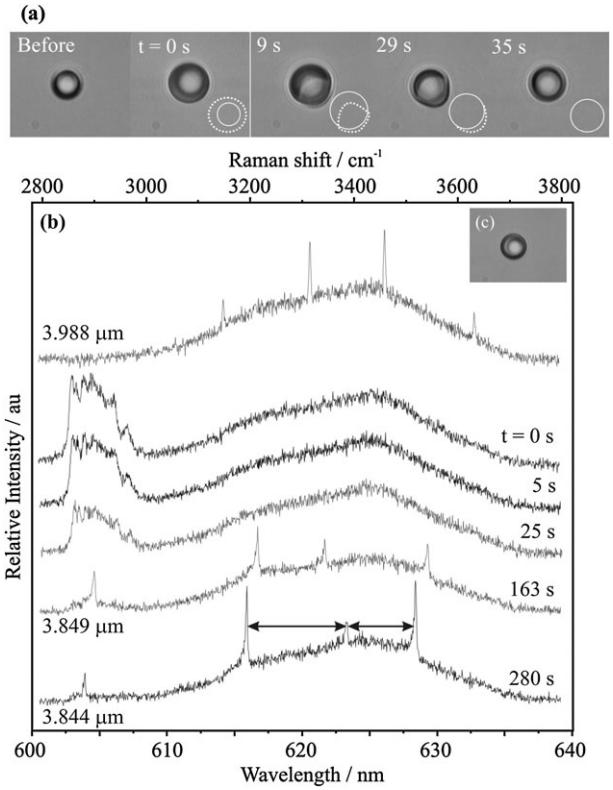

Fig. 9 (a) In-plane images showing the temporal evolution of the multiphase structure of a decane/NaCl/aqueous aerosol droplet following coagulation of a decane droplet with a NaCl/aqueous droplet. The schematic highlights the approximate phase boundaries observed, with the dotted line and the solid line defining the decane phase and the aqueous phase, respectively. [Reprinted with permission from ref. 42. Copyright 2007 American Chemical Society.] (b) Time dependent evolution of the CERS fingerprint following coagulation of a decane droplet with an optically trapped NaCl/aqueous aerosol droplet. The mode offset is defined as the magnitude of the difference between the splittings between TE and TM modes indicated by the arrows. (c) In-plane image of a mixed phase decane/NaCl/aqueous aerosol droplet showing complete engulfing of a water droplet within a host decane droplet. [Reprinted with permission from ref. 22. Copyright 2007 American Chemical Society.]

the effect of organics on aerosol hygroscopicity to be investigated directly.

IV.d Coagulation of immiscible components

Coagulation influences the mixing state of different chemical components present in an aerosol sample. Indeed, the mixing state of an aerosol droplet has a significant impact on its chemical and physical properties. For example, the presence of an inclusion can affect an aerosol's light scattering properties, while the formation of a thin organic layer on an aqueous aerosol droplet's surface can affect the partitioning of a species between the condensed and gas phases. The formation of a multiphase aerosol droplet and the spatial and temporal evolution in mixing state, composition and particle size can be investigated by coupling optical tweezers with CERS. The evolving CERS fingerprint following coagulation can provide information on the mixing state of composite organic/aqueous aerosol droplets and on the degree of phase segregation, recorded with a time resolution of 1 second.

The phase segregation of immiscible organic and aqueous components within a single aerosol droplet was investigated by coagulating a decane droplet with a NaCl/aqueous droplet and monitoring the subsequent temporal evolution in mixing state.[22,23,42] The equilibrium structures of the mixed phase organic/aqueous aerosol can be predicted from a model developed by Torza and Mason, which describes the equilibrium configuration observed when two immiscible phases are brought into contact within a third immiscible phase, in this case the gas phase.[43] The configuration of the multiphase aerosol droplet is dependent upon the volume ratios of the decane and aqueous phases, and the surface and interfacial tensions of each component.[42] The final equilibrium configuration of the three-phase system (decane, water and air) corresponds to the structure with minimum surface energy. Three broad classifications of phase segregated structures can be distinguished: complete engulfing, partial engulfing and non-engulfing. Fig. 9(a) shows the temporal dependence of a

decane/NaCl aqueous droplet following a coagulation event. At the point of coagulation the decane phase completely engulfs the aqueous phase. However, evaporation of the organic component from the droplet results in the translation of the phase boundary and the observation of a partially engulfed structure. This change in configuration is a result of a decreasing decane volume which becomes smaller than the aqueous phase volume.

The time evolution in the CERS fingerprint, observed prior to and following coagulation of a decane droplet with an optically trapped NaCl/aqueous aerosol droplet, is shown in Fig. 9(b).[22] Initially the CERS fingerprint shows the characteristic OH stretching vibration of water with SRS superimposed. Following coagulation of the aqueous droplet with the decane droplet, a clear phase boundary becomes apparent between the two components. The presence of the organic component within the droplet is also evident through the appearance of the CH stretching vibrations in the region 603–605 nm. The SRS is quenched as a result of the presence of the decane phase, which creates a refractive index inhomogeneity within the aqueous droplet, disrupting the circulation of the WGMs and affecting their mode quality.[40] The phase segregation of the aqueous and decane phases can also be confirmed by examining the OH band shape, which reflects the hydrogen bonding environment of the aqueous phase.[22] The similarity of the OH band shape of the composite droplet and that of an aqueous droplet suggests that the hydrogen-bonding environment in the mixed phase droplet is comparable with that in an aqueous water droplet, confirming that the decane and aqueous components are phase separated.

Further, it is important to note that the trapping beam has a cross-section at focus that is smaller than the diameter of the droplet. Thus, any compositional measurement from spontaneous Raman scattering provides a signature of the composition only through the centre of the droplet. This allows the evolution in phase partitioning of the composite droplet to be probed with spatial resolution after the coagulation event.[22] Following coagulation, the decane phase, which is comparable in volume to the aqueous phase, excludes water from the probe volume of the trapping beam. Consequently the CH spontaneous intensity exceeds the OH spontaneous intensity. The evaporation of decane leads to a decrease in the inclusion size, water is no longer excluded from the probe volume, and the OH spontaneous band increases in intensity.

SRS can be used to probe multiphase aerosol droplets which have adopted a core–shell structure consisting of an aqueous droplet core coated in an organic layer, as shown in Fig. 10(a).[44] By comparison of the WGM wavelengths with Mie scattering calculations for a core–shell structure, the aqueous core radius and the shell thickness can be estimated with approaching nanometre accuracy. Further, the evolution of the organic layer thickness, and the effect of layer thickness on aerosol hygroscopicity can be interrogated with high time resolution.

The spacing between a TM mode and adjacent TE modes observed in a CERS fingerprint can provide a signature of the formation of a core–shell structure by a multiphase organic/aqueous droplet. The offset in wavelength of a TM mode from the central wavelength between two adjacent TE modes is approximately invariant with change in size of a homogeneous droplet.[23] The mode offset is defined in Fig. 9(b). However, this mode offset can vary considerably during the growth or evaporation of a layer of different refractive index upon the droplet surface.[45] Fig. 10(b) shows the variation in mode offset calculated for a core–shell droplet with a 3 μm NaCl/aqueous core surrounded by a decane shell of thickness between 0–1 μm.[44] The mode offset is initially close to that of a homogeneous NaCl/aqueous droplet, increasing to a maximum at a layer thickness of 0.2 μm and tending towards that of a homogeneous decane droplet in the limit of a thick shell. With such a thick layer, the WGMs circulate only within the

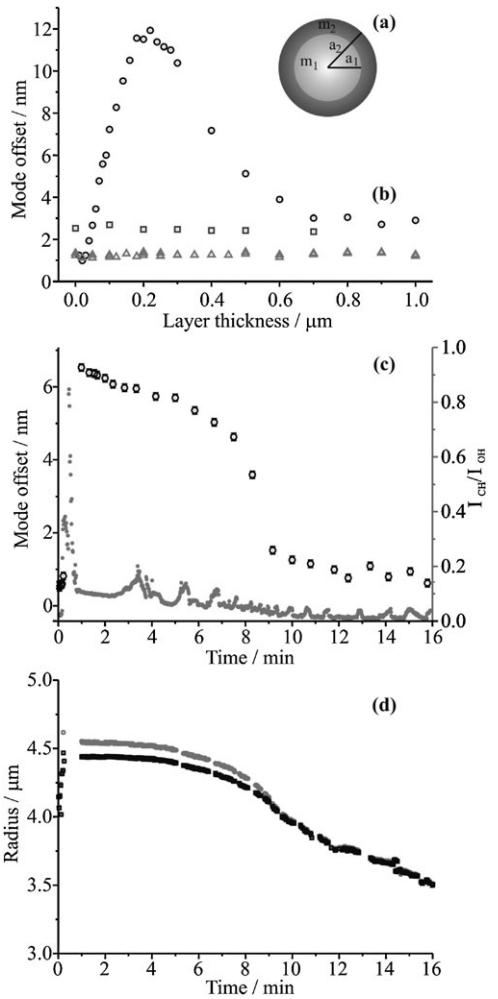

Fig. 10 (a) Schematic of a core–shell droplet composed of a core of refractive index m_1 and radius a_1, surrounded by a layer of refractive index m_2. The total droplet radius equals a_2. (b) Variation in the calculated mode offset for an aqueous/NaCl core of radius 3 μm coated in a decane layer of increasing thickness (circles). The mode offsets observed for a homogeneous NaCl/aqueous aerosol droplet (triangles) and a homogeneous decane droplet (squares) are shown for comparison. (c) Temporal variation in the mode offset (open black circles and left hand axis) and the CH to OH spontaneous band intensity ratio (closed grey circles and right hand axis) observed following coagulation of a decane droplet with a NaCl/aqueous droplet. (d) Temporal evolution of the core (black) and total droplet (grey) radii following the coagulation event. [Reprinted with permission from ref. 44. Copyright 2007 American Chemical Society.]

decane layer and no longer propagate into the aqueous core. For larger droplets, for example those with a radius in excess of 5 μm, the second order modes must also be considered, as these penetrate a greater distance into the droplet bulk and can therefore be used to probe thicker shells.

At long times following the coagulation of a decane and NaCl/aqueous aerosol droplet, WGMs reappear in the CERS fingerprint (Fig. 9(b)), SRS again surpasses threshold and it can be inferred that the droplet has regained some degree of homogeneity. WGMs of the same mode progression are observed to extend over the wavelength range of the OH and CH Raman bands, even though the CH spontaneous band is no longer evident in the CERS fingerprint, indicating the decane and water are both present within the volume from which the signal arises. A possible explanation is that the residual decane has formed a surface layer on the aqueous droplet surface, and the multiphase droplet has adopted a core–shell structure.

By monitoring the evolution in the CERS fingerprint the change in layer thickness can be investigated directly. Fig. 10(c) shows the temporal variation in mode offset following the reappearance of the WGMs. At short times the mode offset is large indicating the presence of a decane layer on the droplet surface. However, it decreases rapidly after 7 minutes suggesting the loss of decane into the gas phase and a decrease in the layer thickness.[44] The loss of decane is confirmed by the decrease of the CH to OH spontaneous band intensity ratio with time. Mie scattering calculations were performed for a core–shell structure, assuming a core refractive index of aqueous NaCl and a shell refractive index of decane. The predicted resonance wavelengths were compared with the observed spectra and the best-fit core size and shell thickness estimated.[44] Fig. 10(d) shows the variation in the core radius and total droplet radius with time. Following evaporation of the decane layer the total droplet radius is observed to tend towards that of the core.

The data suggest that the decane layer has an impact on the evaporation of water from the NaCl/aqueous core.[44] As the layer thickness decreased, the rate of evaporation of the aqueous core was observed to increase, an inverse correlation which suggests that the organic layer may act as a barrier to mass transfer between the condensed phase and the gas phase. These results show the CERS fingerprint can be used to probe the evolving composition and structure of a multiphase aerosol droplet following coagulation of two immiscible aerosol droplets, with high temporal and spatial resolution. The formation of the multiphase aerosol droplet can be monitored directly and in real time, and layer thicknesses can be determined with an accuracy of ±8 nm.

An analogous strategy can be used to characterise the transition from a liquid droplet to a solid particle.[41] As a benchmark example we have investigated the formation of an organic gel particle following the coagulation of an aqueous sodium chloride droplet with a droplet containing a high concentration of the surfactant sodium dodecyl sulfate (SDS). As the water evaporates from the coagulated droplet, micelle structures form aggregates creating an extended metastable gel with occluded water, as shown by the in-plane images in Fig. 11(a–e). In the majority of cases the inhomogeneous aggregates inhibit the formation of WGMs, quenching the SRS and the formation of the solid aerosol droplet can be directly monitored. However, on some occasions, as illustrated by Fig. 11(b) the imhomogeneity in refractive index is not sufficient to quench the SRS. Not only do these measurements suggest that non-spherical particles can be retained in the optical trap, but they suggest that phase transitions can be examined.

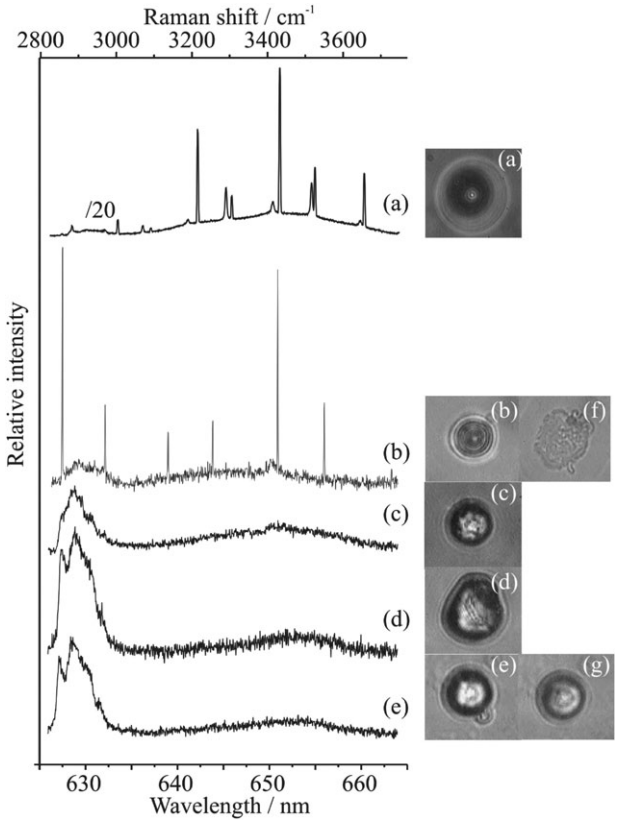

Fig. 11 Images of SDS/NaCl/aqueous droplets of varying composition and phase and corresponding CERS fingerprints: (a) homogeneous liquid-phase; (b) microgel phase with occluded water for which the WGMs were not quenched with (f) the resulting image once the particle is allowed to settle to the coverslip; (c) and (d) further examples of the microgel phase; (e) a large microgel particle with a small particle attached to its surface, following which the smaller particle separates, as shown in (g). [Reprinted with permission from ref. 41. Copyright 2007 American Chemical Society.]

IV.e Heterogeneous reactions in aerosol droplets

Optical tweezers coupled with Raman spectroscopy can be used to study atmospherically important heterogeneous chemistry, as illustrated by King *et al.* who used the technique to investigate the oxidation of aerosol droplets.[46,47] Chemical kinetics measurements were performed by probing the disappearance of reactants in a single droplet during the oxidation of benchmark unsaturated organic compounds following exposure to a flow of ozone in the gas phase over timescales of minutes. Rate constants were evaluated for the oxidation reactions of fumarate or benzoate ions in aqueous droplets, which mimic organic matter found within the atmosphere, and

for the reaction of α-pinene in dodecane or pentadecane droplets, a proxy for biogenic aerosols.[46]

The evolution in droplet size and composition following exposure of the droplet to ozone were monitored using optical microscopy and Raman spectroscopy, respectively. Raman spectroscopy was used to monitor the temporal loss of the reactants and the formation of the products during oxidation, allowing the kinetics of the reaction and the uptake coefficient of the gaseous oxidant, ozone, to be determined in real time. This procedure allowed the heterogeneous condensed phase-gas phase chemical reaction of a single aerosol particle to be studied in real time. Single particle kinetic studies avoid the averaging of results observed for bulk aerosol samples allowing the determination of the rate coefficient between ozone and unsaturated organic components directly.

V. Summary

We have shown that optical tweezers provide a powerful new approach to study the properties of single and multiple aerosol particles. The optical gradient force provides a potential well that tightly confines the particle and allows the robust manipulation of single micron-sized particles held within a gas flow, ensuring particles are retained even during coagulation with other aerosol particles. Multiple aerosol particles can be manipulated and analysed using simple beam-steering optics, an acousto-optic modulator or a spatial light modulator for the formation of holographic arrays of optical traps. When coupled with an array of spectroscopic probes, the evolving size, composition, phase and refractive index of multiple particles can be interrogated with high time-resolution. A direct and concurrent comparison of two particles of different composition exposed to the same gas phase can allow highly accurate comparative measurements of the thermodynamic properties of the two particles or the kinetics of particle growth. Phase segregation within a single multiphase particle can be probed and the formation of mixed phase core–shell droplets inferred. Solid particles can be retained and manipulated with the optical field. Finally, the application of optical tweezers to studies of heterogeneous aerosol chemistry has been described.

Although we have discussed the versatility of the aerosol optical tweezers strategy, there remain some clear challenges. The loading of the optical traps is an uncontrolled process and coagulation between trapped droplets and those passing within the aerosol stream is unavoidable. A method for the controlled and selective loading of optical traps will greatly improve the robustness of the approach, allowing greater control over the droplet composition and size. Further, sizes are currently characterised from the CERS fingerprint which precludes accurate size determination for droplets smaller than $\sim$2.5 μm in radius. The CERS spectra are acquired with 1 second time-resolution and to improve temporal resolution it will be necessary to implement elastic scattering techniques to resolve size changes. Based on the images collected, particles as small as 1 μm diameter have been trapped and manipulated. Reducing this lower size limit would provide a unique opportunity to investigate the properties of particles with increasing surface-to-volume ratio. Finally, trapping solid particles remains challenging; improving the efficiency with which solid particles can be trapped would allow detailed measurements of phase transformation and particle aggregation.

Despite the challenges described above, aerosol optical tweezers are set to play a significant role in improving our understanding of the role of aerosol in a range of complex environments and applications. Key advances will come from the direct comparison of mass accommodation coefficients for the adsorption of trace gas species on liquid–gas surfaces of different composition and the influence of organic components, water soluble and insoluble, on the thermodynamic properties of aerosol. The ability to perform comparative wavelength-resolved measurements of the light absorption efficiency of aerosol containing different absorbing components will allow rigorous testing of the models for calculating the light extinction properties of multicomponent/multiphase aerosol. Finally, the manipulation of arrays of aerosols could provide new analytical techniques for assaying and analysing samples, as well as for performing chemistry, in picolitre volumes.

Acknowledgements

We acknowledge the EPSRC and NERC for financial support and for supporting LM during this work. JPR also acknowledges the EPSRC for support through the award of an Advanced Research Fellowship. Dr David McGloin and Mr. Michael Summers are thanked for helpful discussions and for providing images for Fig. 3.

References

1 J. H. Seinfeld and S. N. Pandis, *Atmospheric Chemistry and Physics: From Air Pollution to Climate Change*, John Wiley & Sons, New York City, 1998.
2 E. J. Davis, *Aerosol Sci. Technol.*, 1997, **26**, 212.
3 C. Marcolli, B. P. Luo and T. Peter, *J. Phys. Chem. A*, 2004, **108**, 2216.
4 A. K. Y. Lee, T. Y. Ling and C. K. Chan, *Faraday Discuss.*, 2008, **137**, 245.
5 M. Schwell, H. Baumgartel, I. Weidinger, B. Kramer, H. Vortisch, L. Woste, T. Leisner and E. Ruhl, *J. Phys. Chem. A*, 2000, **104**, 6726.
6 A. L. Yarin, G. Brenn, O. Kastner and C. Tropea, *Phys. Fluids*, 2002, **14**, 2289.
7 N. J. Mason, E. A. Drage, S. M. Webb, A. Dawes, R. McPheat and G. Hayes, *Faraday Discuss.*, 2008, **137**, 367.
8 A. Ashkin and J. M. Dziedzic, *Appl. Phys. Lett.*, 1971, **19**, 283.
9 R. Thurn and W. Kiefer, *Appl. Opt.*, 1985, **24**, 1515.
10 N. Jordanov and R. Zellner, *Phys. Chem. Chem. Phys.*, 2006, **8**, 2759.
11 J. Popp, M. Lankers, K. Schaschek, W. Kiefer and J. T. Hodges, *Appl. Opt.*, 1995, **34**, 2380.
12 P. Bartlett, Optical Manipulation, in *Colloid Science*, ed. T. Cosgrove, Blackwell publishing Ltd, 2005, p. 255.
13 J. E. Molloy and M. J. Padgett, *Contemp. Phys.*, 2002, **43**, 241.
14 A. Ashkin, J. M. Dziedzic, J. E. Bjorkholm and S. Chu, *Opt. Lett.*, 1986, **11**, 288.
15 R. J. Hopkins, L. Mitchem, A. D. Ward and J. P. Reid, *Phys. Chem. Chem. Phys.*, 2004, **6**, 4924.
16 L. Mitchem, J. Buajarern, R. J. Hopkins, A. D. Ward, R. J. J. Gilham, R. L. Johnston and J. P. Reid, *J. Phys. Chem. A*, 2006, **110**, 8116.
17 K. J. Knox, J. P. Reid, K. L. Hanford, A. J. Hudson and L. Mitchem, *J. Opt. A: Pure Appl. Opt.*, 2007, **9**, S180.
18 R. Omori, T. Kobayashi and A. Suzuki, *Opt. Lett.*, 1997, **22**, 816.
19 N. Magome, M. I. Kohira, E. Hayata, S. Mukai and K. Yoshikawa, *J. Phys. Chem. B*, 2003, **107**, 3988.

20 R. Di Leonardo, G. Ruocco, J. Leach, M. J. Padgett, A. J. Wright, J. M. Girkin, D. R. Burnham and D. McGloin, *Phys. Rev. Lett.*, 2007, **99**, 010601.
21 E. Fallman and O. Axner, *Appl. Opt.*, 1997, **36**, 2107.
22 L. Mitchem, J. Buajarern, A. D. Ward and J. P. Reid, *J. Phys. Chem. B*, 2006, **110**, 13700.
23 J. Buajarern, L. Mitchem, A. D. Ward, N. H. Nahler, D. McGloin and J. P. Reid, *J. Chem. Phys.*, 2006, **125**, 114506.
24 D. McGloin, *Philos. Trans. R. Soc. London, Ser. A*, 2006, **364**, 3521.
25 J. Leach, K. Wulff, G. Sinclair, P. Jordan, J. Courtial, L. Thomson, G. Gibson, K. Karunwi, J. Cooper, Z. J. Laczik and M. J. Padgett, *Appl. Opt.*, 2006, **45**, 897.
26 D. R. Burnham and D. McGloin, *Opt. Express*, 2006, **14**, 4175.
27 D. McGloin, D. R. Burnham, M. D. Summers, D. Rudd, N. Dewar and S. Anand, *Faraday Discuss.*, 2008, **137**, 335.
28 M. D. Summers, J. P. Reid and D. McGloin, *Opt. Express*, 2006, **14**, 6373.
29 D. McGloin and K. Dholakia, *Contemp. Phys.*, 2005, **46**, 15.
30 J. P. Reid and L. Mitchem, *Annu. Rev. Phys. Chem.*, 2006, **57**, 245.
31 J. Popp, M. Lankers, M. Trunk, I. Hartmann, E. Urlaub and W. Kiefer, *Appl. Spectrosc.*, 1998, **52**, 284.
32 R. Symes, R. M. Sayer and J. P. Reid, *Phys. Chem. Chem. Phys.*, 2004, **6**, 474.
33 J. P. Reid, H. Meresman, L. Mitchem and R. Symes, *Int. Rev. Phys. Chem.*, 2007, **26**, 139.
34 L. Mitchem, R. J. Hopkins, J. Buajarern, A. D. Ward and J. P. Reid, *Chem. Phys. Lett.*, 2006, **432**, 362.
35 S. C. Hill and R. E. Benner, Morphology-Dependent Resonances, in *Optical Effects Associated with Small Particles*, ed. P. W. Barber and R. K. Chang, World Scientific, Singapore, 1988.
36 A. J. Campillo, J. D. Eversole and H. B. Lin, *Optical Processes in Microcavities*, World Scientific, Singapore, 1996.
37 J. D. Eversole, H. B. Lin, A. L. Huston, A. J. Campillo, P. T. Leung, S. Y. Liu and K. Young, *J. Opt. Soc. Am. B*, 1993, **10**, 1955.
38 R. M. Sayer, R. D. B. Gatherer, R. J. J. Gilham and J. P. Reid, *Phys. Chem. Chem. Phys.*, 2003, **5**, 3732.
39 J. R. Butler, L. Mitchem, K. L. Hanford, L. Treuel and J. P. Reid, *Faraday Discuss.*, 2008, **137**, 351.
40 H. B. Lin, A. L. Huston, J. D. Eversole, A. J. Campillo and P. Chylek, *Opt. Lett.*, 1992, **17**, 970.
41 J. Buajarern, L. Mitchem and J. P. Reid, *J. Phys. Chem. A*, 2007, **111**, 13038.
42 J. Buajarern, L. Mitchem and J. P. Reid, *J. Phys. Chem. A*, 2007, **111**, 9054.
43 S. Torza and S. G. Mason, *J. Colloid Interface Sci.*, 1970, **33**, 67.
44 J. Buajarern, L. Mitchem and J. P. Reid, *J. Phys. Chem. A*, 2007, **111**, 11852.
45 J. L. Huckaby and A. K. Ray, *Langmuir*, 1995, **11**, 80.
46 M. D. King, K. C. Thompson, A. D. Ward, C. Pfrang and B. R. Hughes, *Faraday Discuss.*, 2008, **137**, 173.
47 M. D. King, K. C. Thompson and A. D. Ward, *J. Am. Chem. Soc.*, 2004, **126**, 16710.